Title

Weak Exciton–Phonon Coupling in CdSe Nanoplatelets from Quantitative Resonance Raman Intensity Analysis

Journal

The Journal of Physical Chemistry C, 122(47)

ISSN

1932-7447

Authors

Maddux, Cassandra JA
Kelley, David F
Kelley, Anne Myers

Publication Date

2018-11-29

DOI

10.1021/acs.jpcc.8b10125

Weak Exciton-Phonon Coupling in CdSe Nanoplatelets from Quantitative Resonance Raman Intensity Analysis

Cassandra J. A. Maddux, David F. Kelley and Anne Myers Kelley*

Chemistry and Chemical Biology, University of California, Merced, 5200 North Lake Road, Merced, CA 95343

*Corresponding author. Email: amkelley@ucmerced.edu

Abstract

Resonance Raman spectra, cross-sections, and depolarization ratios have been measured for 4.5 monolayer thick CdSe nanoplatelets dispersed in chloroform. Five excitation wavelengths between 514.5 and 476.5 nm were employed. The resonance Raman spectra are dominated by the longitudinal optical (LO) phonon near 201 cm^{-1} and its overtone, as in CdSe quantum dots. The absolute scattering intensity is much higher for excitation on resonance with the sharp, lowest-energy heavy-hole to conduction band transition than with higher energy transitions, decreasing by about a factor of 30 between 514.5 nm and 496.5 nm excitation. The LO phonon overtone is weak directly on resonance with the heavy-hole transition but much stronger at higher excitation energies, a result that is reproduced by simulations of the spectra using standard resonance Raman intensity theory. The absolute Raman cross-sections imply a Huang-Rhys parameter for the LO phonon of about 0.08 on resonance with the lowest heavy-hole transition. This is a factor of 2-3 lower than found previously for CdSe quantum dots. The depolarization ratios on resonance with the lowest heavy-hole excitonic transition are slightly higher than expected for a degenerate, plane-polarized transition even when the local field factors are taken into account.

Introduction

Nanoplatelets (NPLs) are semiconductor nanostructures that have a precisely defined and small thickness in one dimension, typically just a few atomic layers, and are much larger in the other two dimensions. With regard to their optical properties, NPLs are essentially bulk-like in the two large dimensions (almost no quantum confinement) but are strongly quantum confined in the thin dimension. Because the thickness in the quantum confined dimension is constant over most of the NPL, there is very little inhomogeneous broadening of the lowest excitonic transition and their absorption and emission spectra are much sharper than can be achieved with quantum dots (QDs). For this and other reasons there has been an explosion of interest in studying these structures since the synthetic protocols for producing CdSe NPLs were established. NPLs have now been synthesized from several semiconductor materials, both in pure form and as core-shell and core-crown heterostructures, as well as alloys. There are well established synthetic protocols for producing CdSe NPLs with thicknesses of 3.5, 4.5, 5.5, 6.5, 7.5, and 8.5 layers (both faces of the platelet are cadmium-terminated), which have their lowest excitonic absorptions at about 460, 512, 552, 581, 604, and 623 nm, respectively.[1-6] In this work we focus on the 4.5 layer thick structures absorbing near 512 nm.

The optical absorption spectra of CdSe NPLs consist of a very sharp low-energy peak, a broader peak 1000-1300 cm^{-1} to the blue, and a weakly structured continuous absorption at higher energies. The two resolved peaks are attributed to the transitions from the tops of the heavy-hole and light-hole valence bands, respectively, to the bottom of the conduction band,[4] although other transitions must also contribute as discussed below. The heavy-hole transition is very sharp, with a half-width at half-maximum on the low-energy side of only 140-160 cm^{-1}, about 2.5 times narrower than QD samples that are considered highly monodisperse. The narrowness of the absorption and emission spectra of NPLs indicates that the exciton-phonon

coupling (EPC) accompanying the heavy-hole transition must be relatively weak, but it is not obvious simply from the linewidths whether the EPC is smaller in NPLs than in QDs. The weak temperature dependence of the emission linewidth was used to conclude that the EPC in NPLs is greatly reduced compared to the bulk, and single-NPL emission spectra at low temperature reveal weak longitudinal optical (LO) phonon features with small Huang-Rhys parameters of S = 0.02 to 0.06.[7] Femtosecond pump-probe experiments on CdSe/CdS core/shell NPLs yield very small Huang-Rhys parameters of ~0.01 for the acoustic phonons.[8] Low-temperature ensemble emission spectra of CdSe NPLs show two peaks separated by approximately the energy of the longitudinal optical phonon,[4,6,9,10] but there are several reasons why these two peaks cannot reasonably be assigned as the 0⟶0 and 0⟶1 vibronic bands: the intensity ratio between the two peaks depends strongly on the lateral dimensions of the NPL, no peak corresponding to a 0⟶2 transition is observed even when the first two peaks are comparable in intensity, and the energy separation between the two peaks varies by more than the LO phonon energy. Alternative explanations are that these two transitions correspond to p-p and s-s transitions, respectively,[9] or that the lower-energy peak corresponds to emission from a charged exciton (trion).[6]

Resonance Raman intensity analysis has been used to quantify EPC in several QD systems, where inhomogeneous broadening makes a large contribution to the observed electronic spectral width.[11-14] A number of studies have reported resonance Raman spectra of CdSe NPLs, but no quantitative intensity analyses have been performed. Surface enhanced Raman spectra (SERS) of NPLs showed a 6 cm^{-1} downshift in the frequency of the longitudinal optical (LO) phonon relative to the unenhanced Raman spectra, which was attributed to excitation of LO phonons oscillating perpendicular to the plane in the SERS geometry.[15] Comparison of the resonant and nonresonant Raman spectra of three thicknesses of CdSe NPLs, quenched with

benzeneselenol and deposited as films, showed LO phonon shifts implying stronger coupling of the out-of-plane phonons to the resonant excitonic transitions.[16] The LO overtone to fundamental intensity ratio decreased with decreasing NPL thickness, suggesting weaker EPC in the thinner NPLs. Both Raman and infrared spectra of CdSe NPLs and their core/shell and core/crown structures with CdS have been reported.[17] Resonance Raman spectra of CdSe NPL films on copper show both the LO phonon and a low-frequency acoustic phonon near 30 cm^{-1} for the 4.5 layer structures.[18] Notably, none of these Raman experiments were carried out under conditions allowing measurement of the absorption spectra, so there is no assurance that the NPLs retained their structural integrity under the conditions employed to obtain the Raman spectra.

In this paper we present the first quantitative resonance Raman intensity analysis of CdSe NPLs. Working in solution under conditions where the absorption spectrum is not significantly perturbed by the ligands used to quench the strong fluorescence, we measure Raman spectra and resonance Raman quantum yields for 4.5 layer thick NPLs at several excitation wavelengths spanning the heavy-hole and light-hole transitions. Quantitative simulation of the absorption spectra and resonance Raman excitation profiles yields values for the exciton-phonon coupling strength. Resonance Raman depolarization ratios are also measured to gain insight into the optical anisotropy of these materials.

Experimental methods

CdSe nanoplatelets with a thickness of 4.5 layers were synthesized and purified largely as described in refs. 3 and 5. Synthetic details are provided in the Supporting Information. TEM images (see Supporting Information) gave x and y dimensions of 26 ± 2 and 6.2 ± 1.2 nm, respectively. Because of the strong and only slightly Stokes-shifted fluorescence from the as-

synthesized NPLs, in order to perform resonance Raman measurements it was necessary to add ligands capable of quenching the fluorescence. While many ligands are known to quench the fluorescence of CdSe QDs through either electron or hole trapping, finding a suitable quencher for NPLs was difficult because most quenchers caused irreversible changes in the absorption spectra of the NPLs, presumably from some combination of etching and aggregation (see Supporting Information). Of a number of ligands tried, only 4-methylbenzenethiol (MBT) gave effective fluorescence quenching without degrading the NPL absorption spectra. 0.5 mL of 0.1 M MBT in chloroform was added to 1 mL of concentrated NPLs (~1.0 μM), 8.3 mL of chloroform, and 0.2 mL of oleic acid and stirred at room temperature under nitrogen. The quenching occurred quickly and completely and the spectra were stable for a period of hours to days.

The Raman experiments were carried out largely as described in ref. 11. Excitation was provided by a cw argon-ion laser with an average power of 0.2-0.3 mW at the sample, focused with a 10x microscope objective onto the sample contained in a 1 mm cuvette. The cuvette was translated continuously under the laser beam to prevent local heating or accumulation of photoproducts. The integrated areas of the Raman peaks were obtained by first subtracting a smooth fluorescence background from the spectrum and then fitting the remaining spectrum to a sum of peaks having a Voigt lineshape using Origin Pro 2015. Absolute scattering cross-sections were obtained by reference to the 667 cm^{-1} line of the chloroform solvent and depolarization ratios were obtained by using the 263 cm^{-1} and 667 cm^{-1} chloroform lines as internal intensity standards as described previously.[11]

Quantitative analysis of the resonance Raman data requires knowledge of the absorption cross-section of the NPLs and of the concentrations of the NPLs in the chloroform solutions, which can be determined from the measured absorbance and the molar absorptivity. Two

recent studies have experimentally determined the molar absorptivity of CdSe NPLs. Achtstein *et al*.[2] used ICP-AES to measure the Cd concentration of NPL samples whose uv-vis absorption spectra had been measured. They expressed their results in terms of the intrinsic absorption coefficient; applying the appropriate unit conversions, we find $\varepsilon = 0.26 \cdot \mu \cdot (vol\ NPL)$ where μ is the intrinsic absorption in cm^{-1}, $vol\ NPL$ is the volume of the nanoplatelet in nm^3, and ε is the molar absorptivity (peak of heavy-hole exciton) in $M^{-1}\ cm^{-1}$. For 4.5 layer NPLs they found μ = 2.27 x 10^5 cm^{-1}, essentially independent of lateral dimension. Yeltik *et al*.[19] similarly used ICP-OES and ICP-MS to directly determine the amounts of Cd and Se in diluted samples of NPLs whose absorption spectra had been measured. They studied several different lateral dimensions for each thickness and derived empirical relationships between molar absorptivity and the lateral area of the NPL. They found a superlinear dependence of molar absorptivity on lateral area and therefore on volume for a fixed thickness, contrary to Achtstein's linear dependence on volume. Because a superlinear dependence on volume appears unphysical, we have chosen to use Achtstein's values for ε. For our lateral dimensions of 26 x 6.2 nm, the volume is 221 nm^3 and the molar absorptivity at the heavy-hole absorption peak is 1.30 x 10^7 M^{-1} cm^{-1} (absorption cross-section 499 $Å^2$). (Yeltik's curves yield a 36% higher molar absorptivity for our lateral dimensions.) This value was used to determine the concentration of the Raman samples and in the modeling of the absorption spectra and resonance Raman intensities.

Computational methods

The computational simulations of the absorption spectra and resonance Raman intensities were carried out using the methods described in ref. 11, modified for the optical anisotropy in the nanoplatelet system. In quantum dots the optical anisotropy is small, although not zero as demonstrated by the Raman depolarization ratios,[11,13] and we assumed that each excitonic

transition consists of a z-polarized component and a doubly degenerate xy-polarized component with a small energetic splitting. In NPLs there is strong quantum confinement in the z direction and weak quantum confinement in the xy plane, and the spectroscopy is often discussed as if x and y are degenerate. However, our Raman depolarization ratios described below show that this is not the case, which we attribute in part to the different local field factors along the x and y directions for NPLs with aspect ratios of about 4. The effective electric field felt inside the NPL, E_{eff}, is different from the incident (external) field, E_{inc}, by a factor that describes the screening of the electric field by the dielectric constant of the NPL:

$$E_{eff,i} = f_i E_{inc,i} \quad (1)$$

where f_i is the local field factor along direction i. If the NPL shape is approximated as an ellipsoid with three different axes, the local field factor is given by[20]

$$f_i = \frac{1}{1+N_i(\varepsilon/\epsilon_0-1)} \quad (2)$$

where ε and ϵ_0 are the dielectric constants in the semiconductor and in the solvent, respectively, and the "depolarization factor" is defined by

$$N_i = \frac{a_x a_y a_z}{2}\int_0^\infty \frac{ds}{(s+a_i^2)\sqrt{(s+a_x^2)(s+a_y^2)(s+a_z^2)}} \quad (3)$$

where a_x, a_y, and a_z are the three semiaxes of the ellipsoid. For relative semiaxis lengths of 26, 6.2, and 1.37 appropriate for our NPLs, the depolarization factors are 0.0219, 0.156, and 0.814 along x, y, and z, respectively. The real part of the dielectric constant for bulk CdSe near 510 nm (2.43 eV)[21] is a little over 7 while the dielectric constant of chloroform is about 2.1. Therefore ε/ϵ_0 is about 3.4 and the local field factors are 0.99, 0.73, and 0.34 along x, y, and z, respectively. Since the electronic transition strength is proportional to the product of the transition dipole matrix element and the effective internal electric field, we can account for the

local field effect in the absorption and Raman calculations by using an effective transition dipole matrix element that is the product of the actual one and the local field factor.

When the x, y, and z directions are nondegenerate, eqs. (4) of ref. 11 for the parallel and perpendicularly polarized differential Raman cross-sections become

$$\left(\frac{d\sigma_{if}}{d\Omega}\right)_{\parallel} = \frac{\omega_L \omega_S^3}{16\pi^2\hbar^2 c^4 \varepsilon_0^2} \frac{5\Sigma^0 + 2\Sigma^2}{15} \tag{4a}$$

$$\left(\frac{d\sigma_{if}}{d\Omega}\right)_{\perp} = \frac{\omega_L \omega_S^3}{16\pi^2\hbar^2 c^4 \varepsilon_0^2} \frac{\Sigma^2}{10} \tag{4b}$$

where

$$\Sigma^0 = \frac{1}{3}\left|\alpha_{xx} + \alpha_{yy} + \alpha_{zz}\right|^2 \tag{5a}$$

$$\Sigma^2 = \frac{1}{3}\left\{\left|\alpha_{xx} - \alpha_{yy}\right| + \left|\alpha_{xx} - \alpha_{zz}\right| + \left|\alpha_{yy} - \alpha_{zz}\right|\right\}^2 \tag{5b}$$

and the Raman polarizabilities, α_{ii} , are calculated as described in ref. 11.

Results and discussion

Figure 1 shows the absorption spectra of the NPLs in chloroform solution before and after quenching the fluorescence by adding 4MBT. The quenching ligand causes a small red-shift of the absorption spectrum, typical for thiol ligands bound to CdSe nanocrystals, and a slightly increased scattering background for low quencher concentrations and short times (a few hours needed to obtain the Raman spectra), although at longer times or at higher concentrations the quencher caused more pronounced broadening of the spectrum. The Raman excitation wavelengths used are also indicated in the figure.

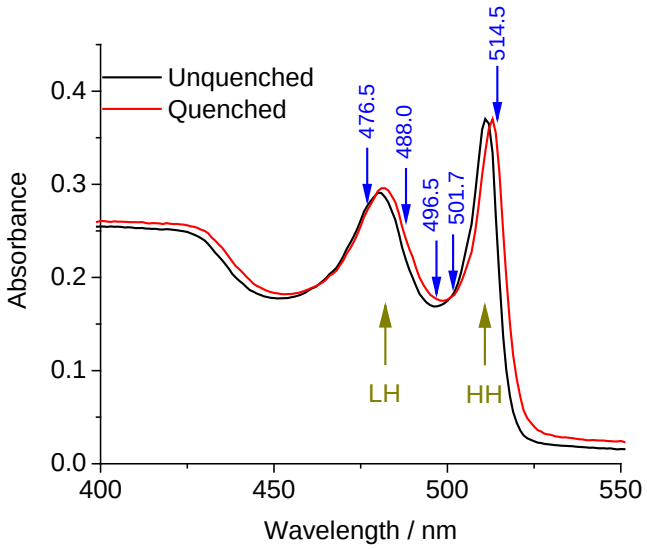

Figure 1. Absorption spectra of original and 4MBT-quenched NPLs. The Raman excitation wavelengths are indicated with blue arrows and the heavy hole (HH) and light hole (LH) transitions are indicated with dark yellow arrows.

Figure 2 shows the resonance Raman spectra of the quenched NPLs at the five excitation wavelengths. Different NPL concentrations were used at different wavelengths in order to keep the LO phonon intensity comparable to that of the major chloroform solvent peaks. The LO fundamental near 201 cm^{-1} is far stronger at 514.5 nm than at any other excitation wavelength. The LO phonon overtone near 407 cm^{-1} is considerably weaker than the fundamental at 514.5 nm excitation, but becomes slightly stronger than the fundamental with 501.7 nm excitation. The NPL Raman spectra at all excitation wavelengths are strongly polarized. Table 1 summarizes the absolute Raman cross-sections for both the LO fundamental and its overtone, the LO fundamental depolarization ratio, and the peak frequencies of the LO fundamental and overtone at all five excitation wavelengths. Figure 3 compares the absorption spectrum with the overtone and fundamental LO Raman cross sections.

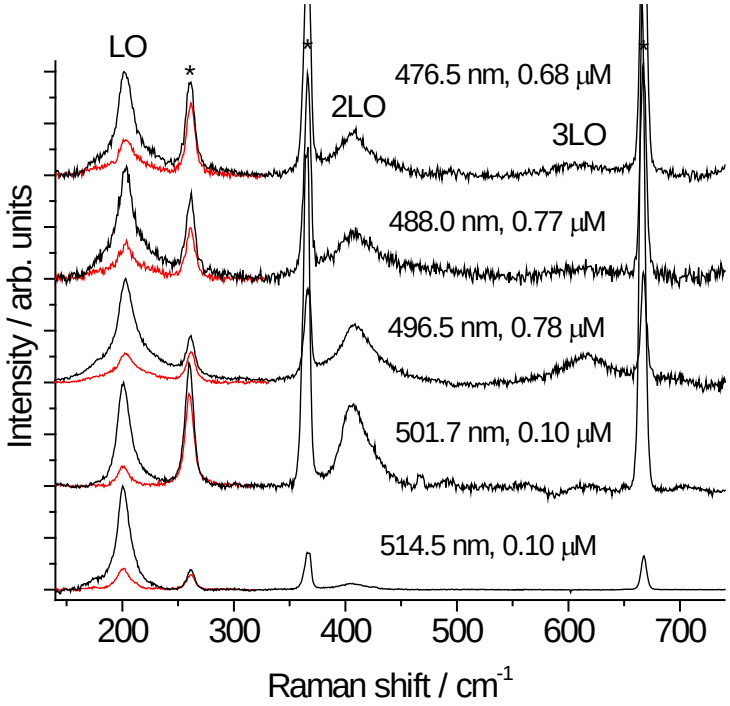

Figure 2. Resonance Raman spectra of CdSe nanoplatelets in chloroform at the indicated concentrations and excitation wavelengths. Parallel polarization data are shown in black and perpendicular polarization are in red (plotted for only the region below 320 cm^{-1}). The fundamental and the first two overtones of the longitudinal optical phonon are labeled (LO, 2LO, 3LO) and asterisks mark solvent lines. Underlying fluorescence backgrounds have been subtracted.

Table 1. Resonance Raman data for CdSe nanoplatelets in chloroform.

exc. wavelength / nm	exc. waveno. / cm^{-1}	LO fund. freq. / cm^{-1}	LO fund. diff. Raman xs $\left(\frac{d\sigma_{if}}{d\Omega}\right)_{\parallel}$ / 10^{-5} Å^2 sr^{-1}	LO overtone freq. / cm^{-1}	LO overtone diff. Raman xs $\left(\frac{d\sigma_{if}}{d\Omega}\right)_{\parallel}$ / 10^{-5} Å^2 sr^{-1}	LO fund. depol. ratio
514.5	19436	200.8±0.6	13.7±4.8	406±2	1.66±0.70	0.23±0.06
501.7	19932	201.8±0.5	1.14±0.33	407±2	1.76±0.62	0.26±0.09
496.5	20141	202.5±0.4	0.43±0.09	409±2	0.33±0.06	0.33±0.08
488.0	20492	202.8±0.4	0.31±0.10	409±2	0.17±0.09	0.39±0.10
476.5	20986	202.5±0.4	0.28±0.08	408±2	0.14±0.06	0.40±0.07

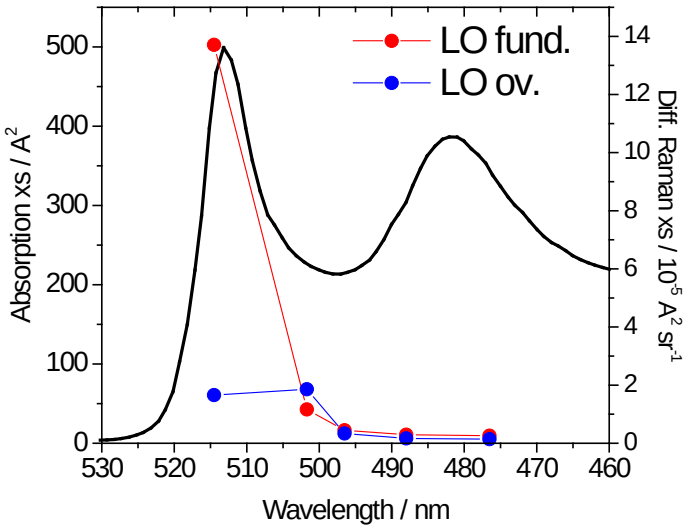

Figure 3. Comparison of experimental absorption spectrum (black) and LO fundamental (red) and overtone (blue) resonance Raman cross sections for CdSe NPLs.

We first discuss the LO fundamental and overtone frequencies. At all excitation wavelengths the LO overtone has its maximum at a frequency somewhat higher than twice the LO fundamental maximum. As positive anharmonicities are unusual, this probably arises from different normal modes contained within the LO phonon band contributing differently to the fundamental and overtone regions. The fundamental peak frequency also appears to vary slightly with excitation wavelength, increasing slightly at higher excitation energies. There is certainly precedent for this; phonon calculations on quantum dots indicate that the "LO phonon" consists of many different, nearly degenerate normal modes that are differentially enhanced at different excitation wavelengths, and this mechanism was invoked to explain the excitation wavelength-dependent LO phonon bandshapes in CdSe quantum dots.[22] However, interpretation of the NPL spectra at shorter excitation wavelengths is clouded by the possibility that the spectra in this region may be contaminated by other species such as QDs. The NPL synthesis always produces some QDs, which are difficult to remove completely while recovering enough material for the Raman measurements. The possible contribution of small CdSe QDs to the NPL Raman spectra at shorter wavelengths can be estimated by referring to our previous QD studies.[13] For CdSe QDs, the peak resonance Raman quantum yield for the LO phonon (defined as the differential Raman cross-section divided by the absorption cross-section at the excitation wavelength), for parallel polarization only, has values of approximately 1.1×10^{-7}, 8.2×10^{-8}, 5.8×10^{-8}, and 4.2×10^{-8} for QDs absorbing at 614, 604, 546, and 510 nm, respectively. Based on these values, we estimate that the Raman yield for QDs absorbing at 470-500 nm should be $2\text{-}4 \times 10^{-8}$. Our apparent measured Raman yields for NPLs at 476.5 and 488.0 nm are roughly two to six times smaller than this. Thus, if QDs contribute only about 10% of the absorbance at these wavelengths, they would contribute roughly 20-40% of the Raman

intensity. This makes us extremely hesitant to proceed with any analysis of the NPL Raman spectra excited at wavelengths shorter than 501.7 nm.

The most dramatic feature evident in Figs. 2 and 3 is the large excitation wavelength dependence of the relative intensities of the LO fundamental and its overtone. The fundamental cross-section drops by nearly an order of magnitude between 514.5 nm, just to the red side of the sharp heavy-hole absorption, and 501.7 nm, in the valley between the heavy-hole and light-hole transitions. It continues to drop at higher excitation energies even through the absorption cross-section remains high. This is similar to what we[11,23] and others[24] have observed in CdSe and CdS quantum dots (QDs) and have attributed largely to destructive interferences among the contributions from multiple, closely spaced excitonic transitions.[23] In contrast, the overtone cross-section is highest at 501.7 nm. This is very different from what is observed in QDs, where the excitation profiles for the overtones are not dramatically different from those of the fundamentals. The large variation in overtone to fundamental intensity ratio in NPLs compared to QDs can be explained qualitatively by the large difference in inhomogeneous broadening in the two systems. For a homogeneously broadened system, the excitation profile for an overtone should peak at a higher energy than the profile for a fundamental because higher vibrational levels of the resonant excited state have relatively better overlaps for the $\Delta v = 2$ transition than for the $\Delta v = 1$ transition. This effect is largely washed out in QDs because of the strong inhomogeneous broadening of the transition, but it is clearly evident in NPLs in which the resonant transition is strong, narrow, and only slightly inhomogeneously broadened.

In order to extract exciton-phonon couplings from the resonance Raman data, it is necessary to computationally simulate the absorption spectrum and the resonance Raman intensities as described in refs. 11 and 13. The inputs to these simulations are the frequency, transition dipole

moment magnitude and direction, homogeneous linewidth, and exciton-phonon coupling strength (Huang-Rhys parameter) for each phonon mode in each excitonic state that contributes to the absorption spectrum and resonance Raman enhancement. This requires making some assumptions about the transitions that compose the absorption spectrum. Simple curve fitting of the experimental spectrum to a sum of Gaussians yields a strong, narrow transition centered near 19480 cm^{-1}, a broader transition with a comparable area centered 200-250 cm^{-1} to the blue, and other peaks at higher energies. The higher-energy part of the spectrum can be fit in a variety of ways that are by no means unique.

The early work of Efros *et al*.[4] assigned the strong, narrow peak near 512 nm and the broader band near 482 nm to the heavy hole/electron and light hole/electron components of the lowest energy exciton, respectively. The heavy hole transition consists of two doubly degenerate excitonic states, $M_J = \pm 2$ and $M_J = \pm 1$. The former are dark and the latter are bright, and they are split by just a few meV.[6] The light hole transition contains four excitonic states, $M_J = \pm 1$ and $M_J = 0$ (two states), all of which have some optically allowed character. The doubly degenerate states are expected to be xy polarized while the nondegenerate transitions are z-polarized.[25] These transitions all result from the fine-structure splitting of the lowest-energy spatial exciton, the one with no nodes. The next lowest-energy spatial exciton should be the p-type exciton that has one node along the x direction of the NPL,[26] and should also be split into heavy-hole and light-hole components having the same polarization behavior as for the lowest exciton.[25] This transition has been assigned to a feature in the low-temperature emission spectrum occurring about 150-300 cm^{-1} to the blue of the lowest excitonic emission depending on lateral dimensions,[9] although other assignments for this feature have also been suggested.[6] Numerous other excitonic transitions should occur at higher energies and contribute to the broad peak traditionally assigned to the light-hole component of the lowest exciton.

For the purposes of modeling both the absorption and resonance Raman spectra we include only the heavy-hole component of the two lowest spatial excitons. This is adequate for reproducing the Raman data excited at 514.5 and 501.7 nm, and for the reasons discussed above we do not attempt to model the higher-energy part of the spectrum. According to Scott *et al*.[25] the heavy hole transitions are xy degenerate, but when we take the local field factors into account, the effective relative transition dipole along the y direction is 74% of that along the x direction. As we expect similar envelope function overlaps for the two lowest spatial excitons, they were assumed to have the same transition dipoles. The lowest exciton was assigned a linewidth that best fits the sharp lowest-energy absorption feature, while the higher transition was assigned a larger linewidth consistent with the increased breadth of the features at higher energies. The best fit is obtained by assuming that the LO phonon has a small Huang-Rhys parameter (S = 0.08) in the lower excitonic state and S = 0 in the higher state, but the conclusion about the higher state is weak because we have not included other, higher-energy transitions that will interfere with it. This value for S is reasonably consistent with the values of S = 0.02 to 0.06 reported by Achtstein *et al*. from single-NPL emission spectra of 5.5 ML structures.[7] Table 2 summarizes the parameters used.

Table 2. Parameters used for modeling CdSe nanoplatelet absorption and resonance Raman spectra. See ref. 11 for a complete description of the parameters.

state	energy / cm^{-1}	linewidth / cm^{-1}	trans. length / $Å^2$, polarization	S
heavy hole (s-type exciton)	19480	240	7.0, x 5.2, y	0.08
heavy hole (p-type exciton)	19680	500	7.0, x 5.2, y	0

Figure 4 compares the calculated and experimental absorption spectra, resonance Raman excitation profiles for both the fundamental and the overtone, and Raman depolarization ratios for the fundamental. This calculation, which assumes that all of the Raman enhancement comes from a single excitonic transition, captures the main features of the data in the region of the heavy-hole exciton. The measured depolarization ratios are somewhat higher than calculated for an xy degenerate transition with the appropriate local field factors. This may reflect out-of-plane distortions of these relatively long and highly flexible NPLs in a room temperature liquid; larger-area NPLs are known to spontaneously roll up to form "nanoscrolls".[27]

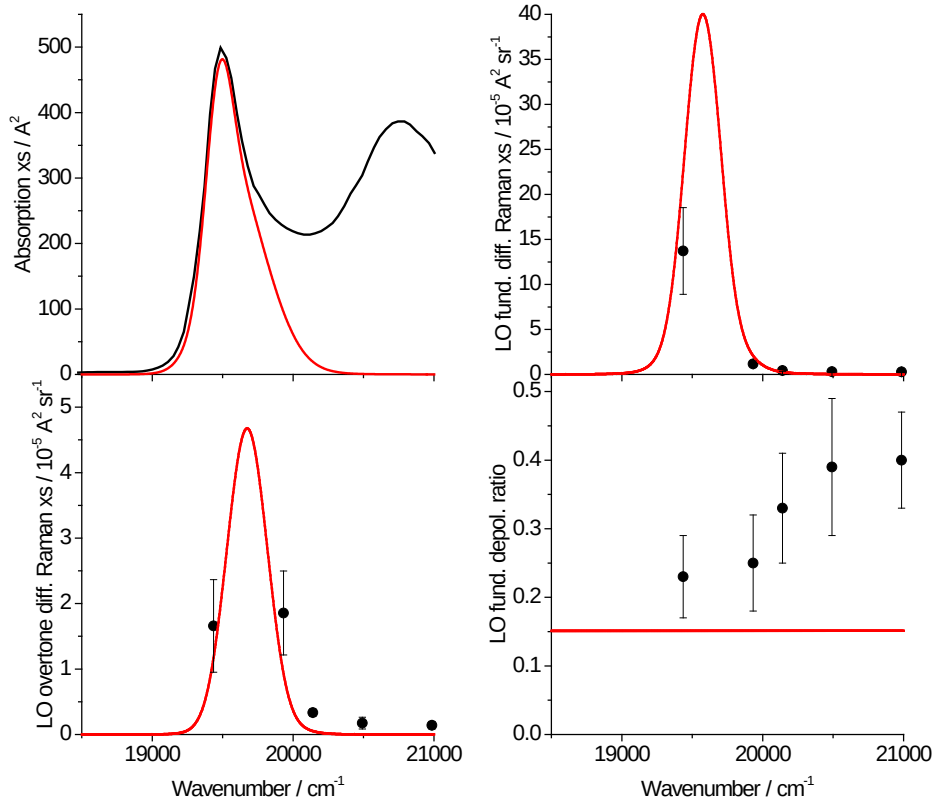

Figure 4. Experimental (black) and calculated (red) absorption cross-section (upper left), differential Raman cross-sections for the LO fundamental (upper right) and LO overtone (lower left), and LO fundamental Raman depolarization ratio (lower right).

The large uncertainties in the experimental cross-sections result mainly from the ambiguity in distinguishing between the bases of the broad Raman peaks and the underlying fluorescence background. Even with the addition of quenching ligands, there is some remaining fluorescence and it is quite structured in the region of the Raman spectrum when exciting at near the heavy-hole transition. It is not clear where to draw the demarcation between Raman and fluorescence, and the Raman line intensities are correspondingly uncertain. Data at each wavelength were obtained for two or more completely different samples and baseline subtraction and peak integration were performed independently by two operators for each sample to obtain the averages and uncertainties for each value. Despite the large error bars, the main features of the data are robust and allow some clear conclusions to be drawn.

In quantum dots, a major contribution to the electronic spectral breadth is the inhomogeneous broadening caused by variations in particle size and shape within the ensemble. Nanoplatelets are unusual in this regard because they exhibit significant quantum confinement in only one dimension (z) and this dimension is very well defined. This is why the heavy-hole transition is so sharp. However, there is certainly some amount of inhomogeneous broadening of the excitonic transitions from incomplete or extra layers near the edges of the NPLs, variations in the lateral dimensions which exhibit small but nonzero quantum confinement, or differences in ligand coverage. We have not included inhomogeneous broadening of the excitonic transitions in our model because we have no way to choose its value. Arbitrarily assuming a small (<100 cm^{-1}) inhomogeneous width requires reducing the homogeneous width of the lowest heavy-hole transition and correspondingly also requires a slightly smaller Huang-Rhys parameter, but does not qualitatively change any of the conclusions.

Resonance Raman spectroscopy allows direct access only to the higher-frequency optical phonons, those above about 100 cm^{-1}. The lower-frequency acoustic phonons are not observable in resonance Raman spectra in room-temperature liquids for several reasons: interference from elastically scattered laser light and from the Rayleigh-Brillouin scattering from the solvent, the expected breadth of these transitions resulting from large thermal populations coupled with some vibrational anharmonicity, and the usual dependence of low-frequency resonance Raman intensities on $S\omega_{ph}^2$.[28] An acoustic mode with a frequency of $\omega_{ph} = 20$ cm^{-1} would be two orders of magnitude weaker than an LO phonon with the same Huang-Rhys parameter. (Acoustic phonons in NPLs have, however, been observed both through frequency-domain Raman spectroscopy in solid films[18] and through ultrafast pump-probe experiments.[8]) Although we do not observe the acoustic phonons directly, their EPC contributes to the overall breadth of the excitonic transition as expressed by the homogeneous linewidth of each transition. The large increase in homogeneous width from the lowest heavy-hole transition to higher-energy transitions may be indicative of stronger coupling to acoustic phonons, but we cannot separate that mechanism from other sources of electronic dephasing or spectral congestion.

The absorption spectrum above 20,000 cm^{-1} is complex and cannot be explained strictly in terms of the heavy-hole and light-hole components of the lowest spatial excitons predicted by a simple particle in a box model. In this simple model the only allowed transitions should be those for which the electron and hole have the same spatial envelope function. For our lateral dimensions and reasonable values of the electron and hole effective masses, the only states that should lie within ~1600 cm^{-1} (0.2 eV) of the lowest exciton are those in which both electron and hole are in the n = 1 level along both the thickness and the width dimensions (y and z), and n = 1 to about 7 along the long axis. However, the breadth and intensity of the absorption indicates that there must be many other contributing transitions in this region. Presumably these are

states in which the electron and hole envelope functions have different quantum numbers along the x direction, but are not orthogonal because the actual potential function is not exactly that of an infinite-walled box. Dozens of such weak transitions should fall within the first ~1600 cm^{-1}. In addition, the single-particle particle-in-box eigenstates are, at best, highly approximate models for the actual excitonic wavefunctions because of the rather strong electron-hole interaction relative to the weak quantum confinement energy along the x and y directions. We conclude that the region of the spectrum traditionally labeled the "light-hole" peak probably consists of a large number of individually rather weak excitonic transitions which are, at present poorly characterized. Fully understanding what these transitions are remains a question for further study.

Conclusions

While several previous papers have discussed the Raman, resonance Raman, and surface-enhanced Raman spectra of CdSe nanoplatelets, this is the first study to make quantitative measurements of the intensities, the first to be carried out in homogeneous solution where the optical absorption spectrum is essentially unperturbed, and the first to relate the measured intensities to a model for the resonant optical transitions. We can state the following conclusions for 4.5 ML CdSe NPLs:

1. The highly structured absorption spectra of NPLs lead to highly structured resonance Raman excitation profiles. Unlike QDs, NPLs exhibit resonance Raman spectra that depend strongly on excitation wavelength and can change rapidly with small variations in resonance condition.

2. The sharp, strong lowest-energy optical transition in CdSe NPLs (heavy-hole component of the lowest-energy spatial exciton) is associated with a small Huang-Rhys parameter for the

longitudinal optical phonon (S ~ 0.08), smaller than that associated with CdSe QDs but close to that previously measured by single-particle emission for 5.5 ML NPLs.

3. The Raman scattering excited on resonance with the lowest-energy exciton is strongly polarized, but somewhat less so than expected for an xy-degenerate exciton even when the anisotropic local field factors are taken into account.

Acknowledgments

This work was supported by NSF grant #CHE-1506803. The TEM images shown in the Supporting Information were obtained with the assistance of Dr. Rui Tan and Prof. Son Nguyen in the laboratory of A. Paul Alivisatos at UC Berkeley.

Supporting Information

Details of the synthetic methods; TEM images of the nanoplatelets; examples of resonance Raman spectra prior to background subtraction. This material is available free of charge via the Internet at http://pubs.acs.org.

(1) Christodoulou, S.; Climente, J. I.; Planelles, J.; Brescia, R.; Prato, M.; Martín-García, B.; Khan, A. H.; Moreels, I. Chloride-Induced Thickness Control in CdSe Nanoplatelets. *Nano Lett.* **2018**, *18*, 6248-6254.

(2) Achtstein, A. W.; Antanovich, A.; Prudnikau, A.; Scott, R.; Woggon, U.; Artemyev, M. Linear Absorption in CdSe Nanoplates: Thickness and Lateral Size Dependency of the Intrinsic Absorption. *J. Phys. Chem. C* **2015**, *119*, 20156−20161.

(3) Achtstein, A. W.; Prudnikau, A. V.; Ermolenko, M. V.; Gurinovich, L. I.; Gaponenko, S. V.; Woggon, U.; Baranov, A. V.; Leonov, M. Y.; Rukhlenko, I. D.; Fedorov, A. V.; Artemyev, M. V.

Electroabsorption by 0D, 1D, and 2D Nanocrystals: A Comparative Study of CdSe Colloidal Quantum Dots, Nanorods, and Nanoplatelets. *ACS Nano* **2014**, *8*, 7678-7686.

(4) Ithurria, S.; Tessier, M. D.; Mahler, B.; Lobo, R. P. S. M.; Dubertret, B.; Efros, A. L. Colloidal Nanoplatelets with Two-Dimensional Electronic Structure. *Nature Mater.* **2011**, *10*, 936-941.

(5) She, C.; Fedin, I.; Dolzhnikov, D. S.; Dahlberg, P. D.; Engel, G. S.; Schaller, R. D.; Talapin, D. V. Red, Yellow, Green, and Blue Amplified Spontaneous Emission and Lasing Using Colloidal CdSe Nanoplatelets. *ACS Nano* **2015**, *9*, 9475–9485.

(6) Shornikova, E. V.; Biadala, L.; Yakovlev, D. R.; Sapega, V. F.; Kusrayev, Y. G.; Mitioglu, A. A.; Ballottin, M. V.; Christianen, P. C. M.; Belykh, V. V.; Kochiev, M. V.; *et al*. Addressing the Exciton Fine Structure in Colloidal Nanocrystals: The Case of CdSe Nanoplatelets. *Nanoscale* **2018**, *10*, 646-656.

(7) Achtstein, A. W.; Schliwa, A.; Prudnikau, A.; Hardzei, M.; Artemyev, M. V.; Thomsen, C.; Woggon, U. Electronic Structure and Exciton–Phonon Interaction in Two-Dimensional Colloidal CdSe Nanosheets. *Nano Lett.* **2012**, *12*, 3151-3157.

(8) Dong, S.; Lian, J.; Jhon, M. H.; Chan, Y.; Loh, Z.-H. Pump-Power Dependence of Coherent Acoustic Phonon Frequencies in Colloidal CdSe/CdS Core/Shell Nanoplatelets. *Nano Lett.* **2017**, *17*, 3312−3319.

(9) Achtstein, A. W.; Scott, R.; Kickhöfel, S.; Jagsch, S. T.; Christodoulou, S.; Bertrand, G. H. V.; Prudnikau, A. V.; Antanovich, A.; Artemyev, M.; Moreels, I.; *et al*. *p*-State Luminescence in CdSe Nanoplatelets: Role of Lateral Confinement and a Longitudinal Optical Phonon Bottleneck. *Phys. Rev. Lett.* **2016**, *116*, 116802.

(10) Biadala, L.; Liu, F.; Tessier, M. D.; Yakovlev, D. R.; Dubertret, B.; Bayer, M. Recombination Dynamics of Band Edge Excitons in Quasi-Two-Dimensional CdSe Nanoplatelets. *Nano Lett.* **2014**, *14*, 1134-1139.

(11) Baker, J. A.; Kelley, D. F.; Kelley, A. M. Resonance Raman and Photoluminescence Excitation Profiles and Excited-State Dynamics in CdSe Nanocrystals. *J. Chem. Phys.* **2013**, *139*, 024702.

(12) Gong, K.; Kelley, D. F.; Kelley, A. M. Resonance Raman Spectroscopy and Electron-Phonon Coupling in Zinc Selenide Quantum Dots. *J. Phys. Chem. C* **2016**, *120*, 29533-29539.

(13) Lin, C.; Gong, K.; Kelley, D. F.; Kelley, A. M. Size Dependent Exciton-Phonon Coupling in CdSe Nanocrystals through Resonance Raman Excitation Profile Analysis. *J. Phys. Chem. C* **2015**, *119*, 7491-7498.

(14) Lin, C.; Gong, K.; Kelley, D. F.; Kelley, A. M. Electron-Phonon Coupling in CdSe/CdS Core-Shell Quantum Dots. *ACS Nano* **2015**, *9*, 8131-8141.

(15) Sigle, D. O.; Hugall, J. T.; Ithurria, S.; Dubertret, B.; Baumberg, J. J. Probing Confined Phonon Modes in Individual CdSe Nanoplatelets Using Surface-Enhanced Raman Scattering. *Phys. Rev. Lett.* **2014**, *113*, 087402.

(16) Cherevkov, S. A.; Fedorov, A. V.; Artemyev, M. V.; Prudnikau, A. V.; Baranov, A. V. Anisotropy of Electron-Phonon Interaction in Nanoscale CdSe Platelets as Seen via Off-Resonant and Resonant Raman Spectroscopy. *Phys. Rev. B* **2013**, *88*, 041303.

(17) Dzhagan, V.; Milekhin, A. G.; Valakh, M. Y.; Pedetti, S.; Tessier, M.; Dubertret, B.; Zahn, D. R. T. Morphology-Induced Phonon Spectra of CdSe/CdS Nanoplatelets: Core/Shell *vs*. Core–Crown. *Nanoscale* **2016**, *8*, 17204-17212.

(18) Girard, A.; Saviot, L.; Pedetti, S.; Tessier, M. D.; Margueritat, J.; Gehan, H.; Mahler, B.; Dubertret, B.; Mermet, A. The Mass Load Effect on the Resonant Acoustic Frequencies of Colloidal Semiconductor Nanoplatelets. *Nanoscale* **2016**, *8*, 13251-13256.

(19) Yeltik, A.; Delikanli, S.; Olutas, M.; Kelestemur, Y.; Guzelturk, B.; Demir, H. V. Experimental Determination of the Absorption Cross-Section and Molar Extinction Coefficient of Colloidal CdSe Nanoplatelets. *J. Phys. Chem. C* **2015**, *119*, 26768−26775.

(20) Sihvola, A. Dielectric Polarization and Particle Shape Effects. *J. Nanomaterials* **2007**, *2007*, 45090.

(21) Ninomiya, S.; Adachi, S. Optical Properties of Cubic and Hexagonal CdSe. *J. Appl. Phys.* **1995**, *78*, 4681-4689.

(22) Lin, C.; Kelley, D. F.; Rico, M.; Kelley, A. M. The "Surface Optical" Phonon in CdSe Nanocrystals. *ACS Nano* **2014**, *8*, 3928-3938.

(23) Gong, K.; Kelley, D. F.; Kelley, A. M. Resonance Raman Excitation Profiles of CdS in Pure CdS and CdSe/CdS Core/Shell Quantum Dots: CdS-Localized Excitons. *J. Chem. Phys.* **2017**, *147*, 224702.

(24) Alivisatos, A. P.; Harris, T. D.; Carroll, P. J.; Steigerwald, M. L.; Brus, L. E. Electron-Vibration Coupling in Semiconductor Clusters Studied by Resonance Raman Spectroscopy. *J. Chem. Phys.* **1989**, *90*, 3463-3468.

(25) Scott, R.; Heckmann, J.; Prudnikau, A. V.; Antanovich, A.; Mikhailov, A.; Owschimikow, N.; Artemyev, M.; Climente, J. I.; Woggon, U.; Grosse, N. B.; *et al*. Directed Emission of CdSe Nanoplatelets Originating from Strongly Anisotropic 2D Electronic Structure. *Nature Nanotechnol.* **2017**, *12*, 1155-1161.

(26) Morgan, D. P.; Maddux, C. J. A.; Kelley, D. F. Transient Absorption Spectroscopy of CdSe Nanoplatelets. *J. Phys. Chem. C* **2018**, *122*, 23772-23779.

(27) Bouet, C.; Mahler, B.; Nadal, B.; Abecassis, B.; Tessier, M. D.; Ithurria, S.; Xu, X.; Dubertret, B. Two-Dimensional Growth of CdSe Nanocrystals, from Nanoplatelets to Nanosheets. *Chem. Mater.* **2013**, *25*, 639-645.

(28) Myers, A. B.; Mathies, R. A. In *Biological Applications of Raman Spectroscopy*; Spiro, T. G., Ed.; Wiley: New York, 1987; Vol. 2, pp 1-58.

Table of Contents graphic